Title:

Cochlear nucleus small cells use olivocochlear collaterals to encode sounds in noise

Adam Hockley[1], Calvin Wu[1], Susan E Shore[1,2,3]

[1] Kresge Hearing Research Institute, Department of Otolaryngology, [2] Department of Molecular and Integrative Physiology, and [3] Department of Biomedical Engineering
University of Michigan, Ann Arbor, MI, 48109, U.S.A.

Correspondence:
Dr. Susan E. Shore,
Department of Otolaryngology, University of Michigan, 1150 West Medical Center Drive, Ann Arbor, MI 48109
sushore@umich.edu

Author contributions:
A.H., C.W. and S.E.S. designed research; A.H. and C.W. performed research; A.H. and CW analyzed data; A.H., C.W. and S.E.S. wrote the paper.

Number of Figures: 7
Number of Tables: 1
Number of words in abstract: 124
Number of words in introduction: 387
Number of words in discussion: 1164

Conflict of Interest Statement: The authors declare that the research was conducted in the absence of any commercial or financial relationships that could be construed as a potential conflict of interest.

Acknowledgements:
The authors would like to thank Mr. Dileepkumar for engineering support throughout this project. This study was supported by National Institutes of Health grant R01-DC017119 (S.E.S.).

ABSTRACT

Understanding speech, especially in noisy environments, is crucial to social interactions. Yet, as we age, speech processing can be disrupted by cochlear damage and the subsequent auditory nerve fiber degeneration. The most vulnerable—medium and high-threshold—auditory nerve fibers innervate various cell types in the cochlear nucleus, among which, the small cells are unique in receiving this input exclusively. Here, we characterize small cell firing characteristics, demonstrating superior temporal as well as intensity coding. We show that small-cell unique coding properties are facilitated by direct cholinergic input from the medial olivocochlear system. These results highlight the small cell–olivocochlear circuit as a key player in signal processing in noisy environments, which may be selectively degraded in aging or after noise insult.

INTRODUCTION

Speech perception in ever-changing soundscapes is key for communication. However, this important task is degraded with age (Pichora-Fuller, 1997). Crucial to speech signal processing are the temporal fine structures and envelope information (Shannon et al., 1995), and difficulties in resolving these signals by the brain can produce speech-in-noise perceptual difficulties (Bharadwaj et al., 2014). In the auditory periphery, the high threshold, low spontaneous rate (SR) auditory nerve fibers (ANFs) may be particularly important as their best dynamic range overlaps with normal levels of communicative signals. These specialized ANFs project along with low threshold ANFs throughout the cochlear nucleus (CN). However, the small-cell cap region receives exclusive input from low (and medium) SR ANFs (Liberman, 1991; Ryugo, 2008).

Located between the granule-cell and magnocellular domains (Cant, 1993), the small-cell cap (SCC), as the name suggests, is a region containing small cells (SCs; <20 µm). SCs project either to medial olivocochlear (MOC) neurons in the ventral nucleus of the trapezoid body (VNTB; Darrow et al., 2012; De Venecia et al., 2005; Thompson & Thompson, 1991; Ye et al., 2000) or directly to the medial geniculate body, the latter serving as short-latency relay to the auditory cortex (Schofield, Mellott, et al., 2014; Schofield, Motts, et al., 2014). SCs, in turn, receive branched collaterals from MOC neurons (Benson et al., 1996; Benson & Brown, 1990; Ryan et al., 1990), whose major function is suppression of cochlear outer hair cell electromotility to alter cochlear gain. MOC activation releases the cochlea from background masking by shifting its dynamic range (Dolan & Nuttall, 1988; Kawase & Liberman, 1993). However, SCs remain largely unexplored. Here, we hypothesize that MOC collateral projections to the CN, and especially onto SCs, may counteract the effect of cochlear suppression, allowing SC firing to accurately represent stimulus intensity.

In this study, we characterized SCs response properties that are consistent with its unique circuit arrangement. We showed that SCs can more accurately encode intensity as well as temporal information compared to other CN cell types. Further, we found both MOC activation and inhibition of cholinergic input to the CN bidirectionally modulated SC firing properties. In the presence of background noise, SCs maintained superior intensity coding. Taken together, these

77 findings reveal a special role for SCs in processing communicative signals and that its degradation
78 after selective auditory neuropathy may underlie speech-in-noise difficulties.

RESULTS

Using multichannel electrodes, we isolated 1523 single units from 83 CN electrode locations in 26 guinea pigs. Unit distributions are shown in Table 1. We excluded onset units in subsequent analyses due to their low numbers.

	PL	Ch	SC	On	B	Total
Control	722	247	310	57	187	1523
VNTB stimulation	260	96	139	15	75	585
Atropine infusion	20	36	34	4	8	102

Table 1: Number of single CN units recorded. Cell types are Primary-like (PL), Chopper (Ch), Small cell (SC), Onset (On) and Buildup (B).

Single-shank 32-channel electrodes with 50 µm spacing of electrode sites were positioned to simultaneously record units from the dorsal CN (DCN), SCC and ventral CN (VCN)(Fig 1). Units were classified by their temporal and frequency response patterns (Fig 1B)(Stabler et al., 1996; Winter & Palmer, 1995; Young et al., 1988). SCs, located dorsoventrally between DCN and VCN, displayed several unusual PSTH shapes, the most common being a 'flat' or bimodal PSTH shape (Fig 1B). SCs were therefore identified by a combination of their PSTH shapes and unique locations within the cochlear nucleus and by their distinct best frequency (BF) progressions with depth.

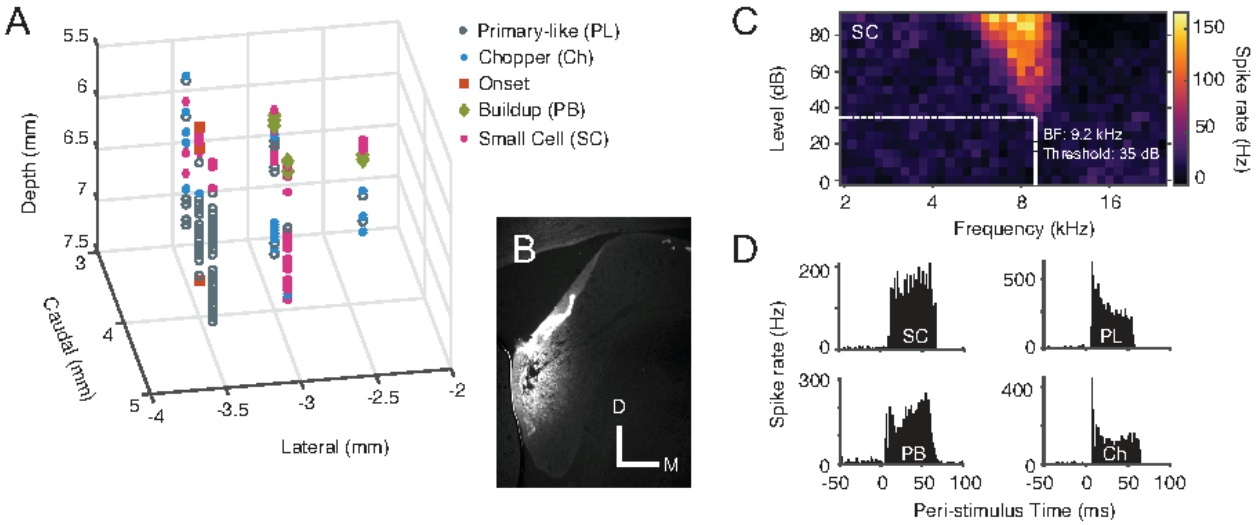

Fig 1: Validating recordings from CN small cells. A) An example 3D plot of unit types within the left CN of one guinea pig. Cells exhibiting buildup PSTH shapes were found more medial and caudal, in the DCN. The VCN is more rostral and lateral, with the SCC units located between these two structures. B) Coronal section of the cochlear nucleus, containing a Fluorogold-marked electrode track in the SCC. (Bar = 0.5 mm) C) Receptive field of a CN small cell. D) Example PSTHs from 4 different CN cell types: small cell (SC) with flat, bimodal PSTH, primary-like (PL), buildup (PB) and chopper (CH).

To confirm reciprocal projections from SCs to MOC neurons in the VNTB, a tracer (FluoroEmerald) was pressure-injected into the VNTB. One week later, retrograde and anterograde staining was observed in the SCC (Fig 2), demonstrating, along with the physiological data, that SCC neurons form a circuit with MOC neurons, confirming previous findings (Benson et al., 1996; Benson & Brown, 1990; Ye et al., 2000).

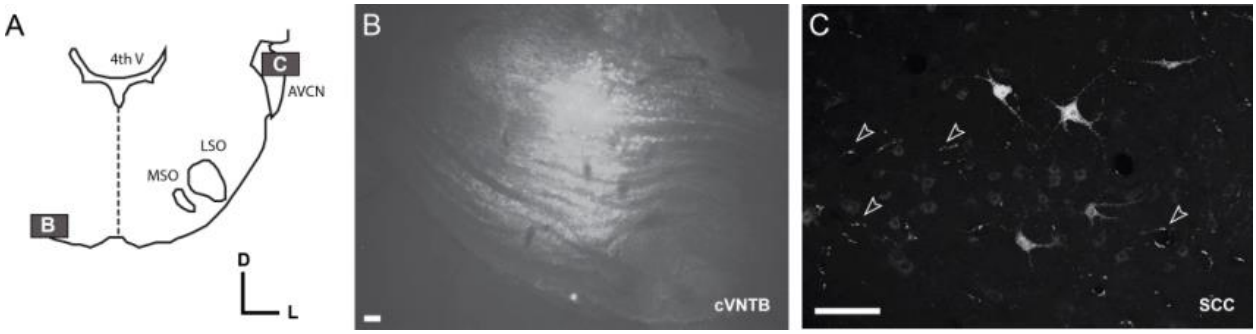

Fig. 2: VNTB neurons project to and receive projections from the SCC. A) Schematic showing the locations of photomicrographs in B (VNTB) and C (SCC). B) FluoroEmerald injection in the contralateral VNTB (cVNTB). C) Anterograde labeling of puncta (arrowsheads) in SCC originating in VNTB and retrograde labelling of SCC somata. Bar = 100 µm.

Small cell firing patterns resemble those of low/medium SR ANFs

Afferent input to SCs is exclusively from low/med SR, high threshold ANFs, while SCs project to, and receive input from MOC neurons. Due to this unique circuit configuration, we hypothesized that SCs would have different patterns of intensity coding (rate-level functions) compared to other CN cell types that also receive input from high SR, low threshold ANFs. SC response characteristics were like their low/medium SR, high threshold ANF inputs, with low SRs, high thresholds, and long first-spike latencies compared to other VCN cell types (Fig S1). SC receptive fields contained inhibitory areas (Figs 1C S1D), signifying a currently unknown source of inhibition. Like low SR ANFs, SCs had non-saturating rate-level functions (RLFs). Above 80 dB SPL, SC RLFs slopes were significantly greater compared to all other CN cell types (Fig 3C).

To examine intensity coding at speech-relevant levels, we used a PSTH-based classifier to compare the trial to trial reliability across cell types in response to different intensity stimuli (Foffani & Moxon, 2004). Intensity coding fidelity is represented by accurate representations of stimuli for each single-trial spiking response (Fig 3D). Primary-like units displayed better intensity discrimination between 20-45 dB as well as very low variability even for misclassified trials, while SCs were better at intensity coding above 60 dB (Fig 3E–F; ANCOVA $F=9.1$, $P=1.1e-4$, effect size (partial eta squared) =0.006). The high-fidelity intensity coding and absence of RLF plateaus in SCs is likely due to their input from low SR ANFs combined with excitatory input from MOCs at high sound levels. The combined action of peripheral and central excitation would allow SCs to better encode tone intensities at levels relevant for speech processing.

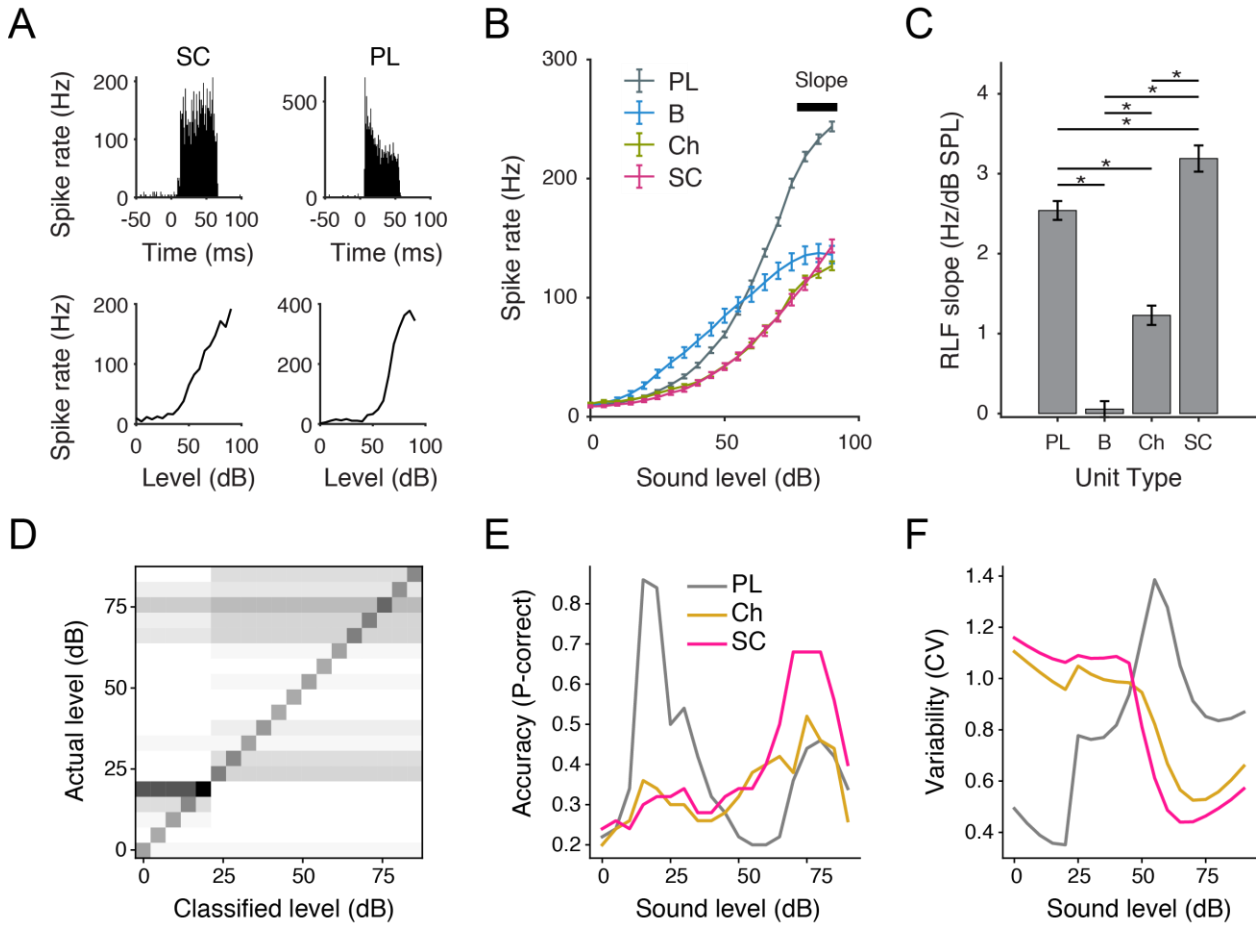

Fig 3: CN small cells show superior intensity coding at high sound levels. A) Example PSTH and RLF for a CN small cell and a primary-like unit. B) Mean (± SEM) RLFs of 4 major CN cell types. 'Slope' marks the region of the RLF used for slope quantification. C) Quantification of RLF slopes between 80- and 90 dB SPL, calculated as the spike rate increase per dB SPL increase (mean ± SEM). Comparisons between groups were made using a Kruskal-Wallis with Tukey's multiple comparison test ($p<0.05$). D) Confusion matrix for sound intensity classification across the population (all cell types). Greyscale – white pixels: 0%, black pixels: 100%. E) Probability of correct classification across unit-types. F) Trial to trial variability (coefficient of variation) of classifier performance across unit-types.

MOC neurons modulate small-cell excitability

Cholinergic MOC neurons send projections into the SCC (Benson et al., 1996; Benson & Brown, 1990; Ryan et al., 1990). Acetylcholine is known to act on CN cells through muscarinic receptors, resulting in a cell-type specific excitation or modulation of neural plasticity (Fujino & Oertel, 2001; Stefanescu & Shore, 2017). To investigate whether cholinergic MOC inputs mediate the steeper RLF slopes in SCs, first, we applied the muscarinic acetylcholine receptor (mAChR) antagonist, atropine using drug delivery probes. Atropine reduced SC tone-evoked activity above 60 dB SPL, confirming a role of cholinergic input in the steepened SC RLF slopes at high tone intensities (Fig 4). Chopper cells, which also receive cholinergic input (Fujino & Oertel, 2001), likewise showed

reduced sound-evoked activity following atropine infusion, but over a narrow intensity range. Atropine had no significant effect on the RLF slopes of primary-like or buildup cells. These findings demonstrate that the primary action of cholinergic input on SCs and choppers is to increase sound-driven responses above 60 dB, resulting in a widened dynamic range that is essential for intensity coding.

Next, to determine whether the MOCs were the key cholinergic modulators of SCs, we electrically stimulated MOC neuron somata in the VNTB while performing CN recordings. Successful targeting of MOC cells was confirmed by the reduction of cochlear compound action potential (CAP) amplitudes during electrical stimulation. MOC stimulation significantly increased SC firing rates to tones above 70 dB SPL but not to lower intensity or sub threshold tones (Fig 4), suggesting that cholinergic MOC input to CN small cells enhances ANF-evoked activity. As expected, the overall effect of MOC activation on CN small cells was opposite to that achieved by cholinergic blocking. In contrast, VNTB stimulation had no effect on chopper firing while decreasing primary-like firing across the entire range of tone intensities. An unexpected finding was an increase in fusiform cell firing rates with MOC stimulation but no effect by blocking muscarinic receptors. The reciprocal findings of increased firing rates with MOC stimulation and decreased firing rates with atropine in SCs confirm the role of MOC input to SCs in enhancing sound-driven responses. Furthermore, SC excitation by MOC neurons can overcome the MOC suppression of cochlear output. The failure of MOC stimulation to alter firing rates in choppers suggests that the cholinergic effect observed originates from VNTB cells that are not MOCs.

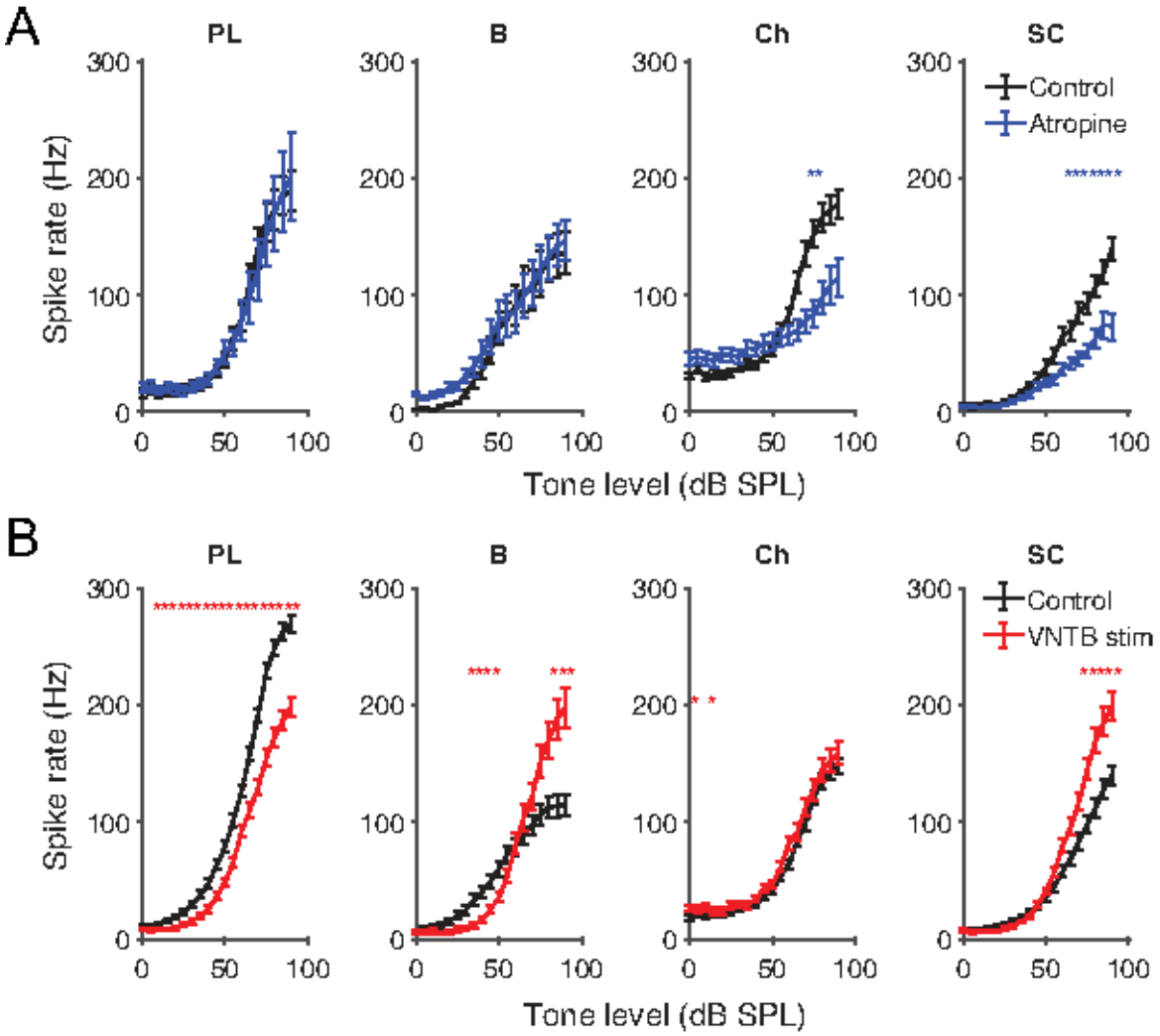

Fig 4: CN small cells receive excitatory cholinergic input from MOCs. Top row: Blocking muscarinic cholinergic receptors with atropine supresses CN small-cell and chopper responses to tones. Top row shows mean RLFs ± SEM for primary-like, buildups, chopper cells and small cells before and after local application of atropine via a drug-delivery probe. Bottom row: Electrically stimulating MOC neurons increases tone-evoked responses in small cells but not choppers. Mean RLFs ±SEM for primary-like, buildups, chopper cells and small cells are shown before and during MOC electrical stimulation. All statistical comparisons made using paired t-test with Bonferroni's multiple comparison correction ($\alpha = 0.00263$, stars signify $p<0.05$).

Small cells use MOC input to precisely encode tones in background noise

MOC projections to the cochlea suppress cochlear outer hair cell electromotility, thereby reducing cochlear amplification. A subsequent unmasking of sounds by background noise facilitates the detection of tones and speech in noise (Dolan & Nuttall, 1988; Kawase & Liberman, 1993). Since SCs receive projections from MOC collaterals, we hypothesized that SCs are involved in encoding sounds in the presence of background noise. Signal-in-noise discrimination was tested in CN neurons by comparing firing rates to tones in silence with tones embedded in broadband noise.

As seen in individual and mean RLFs, SCs maintained their firing rates to tones even in the presence of background noise (Fig 5). In fact, SC spike rates in response to BF tones in the presence of 40- and 60 dB background noise were equivalent to their responses to tones in silence (Fig 6). Chopper units also maintained their firing rates to BF tones in background noise at 40, but not 60 dB SPL. In contrast, background noise degraded the responses to BF tones in primary-like and buildup cells, which showed degraded firing rates in the presence of 40- and 60 dB SPL broadband noise. These differences were not due to thresholds as they were apparent for cells of similar thresholds. Taken together, these results demonstrate that, vis-à-vis other CN cell types, small cells reliably encode medium to high stimulus intensity in the presence of background noise.

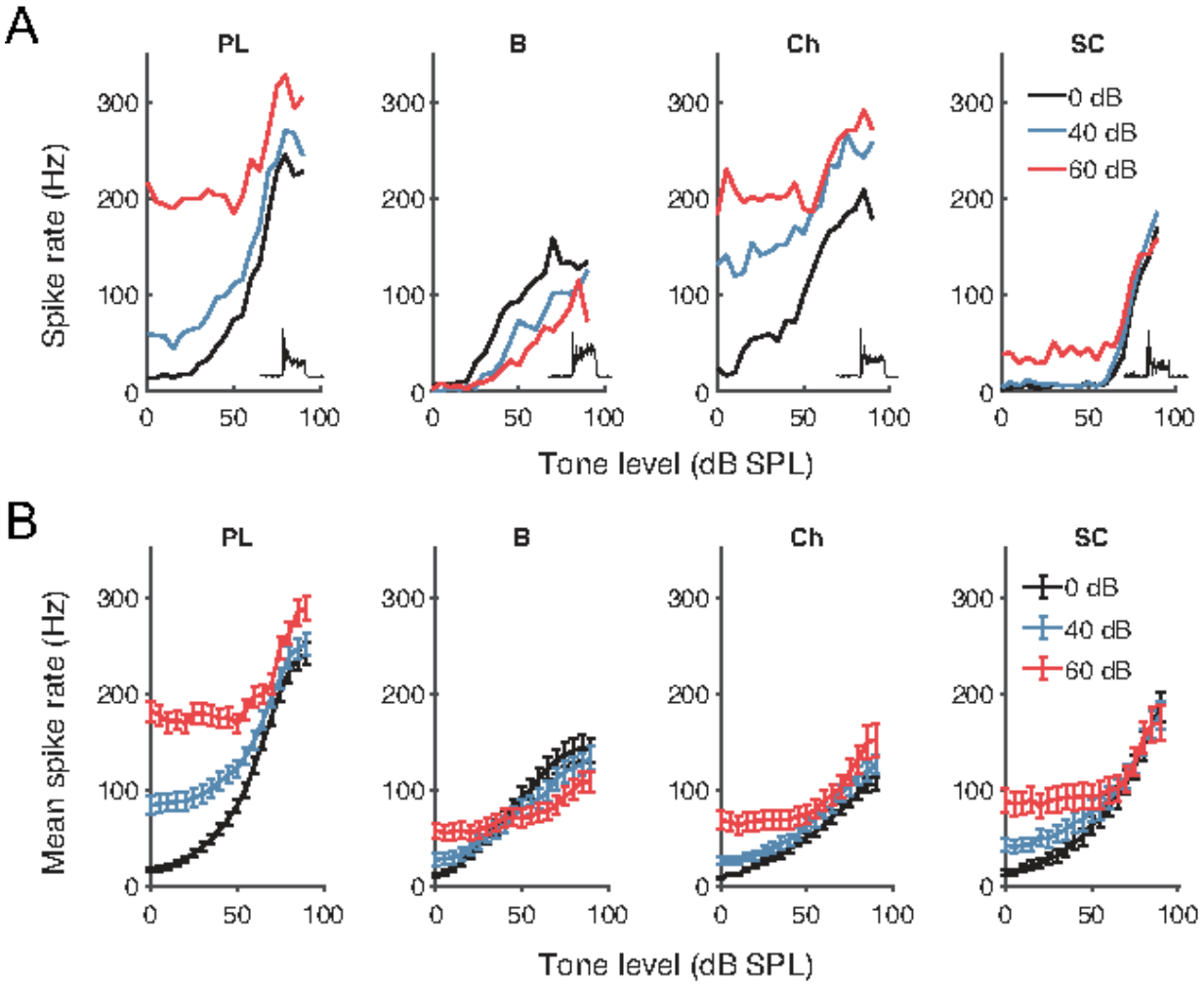

Fig 5: CN small cells maintain tone-level coding in the presence of background noise. A) Single unit examples of RLFs in the presence of 0, 40- or 60 dB SPL background noise, for the 4 major cell-type classifications (columns). Insets show PSTH shapes. B) Mean (± SEM) RLFs of 4 major CN cell types in the presence of background noise.

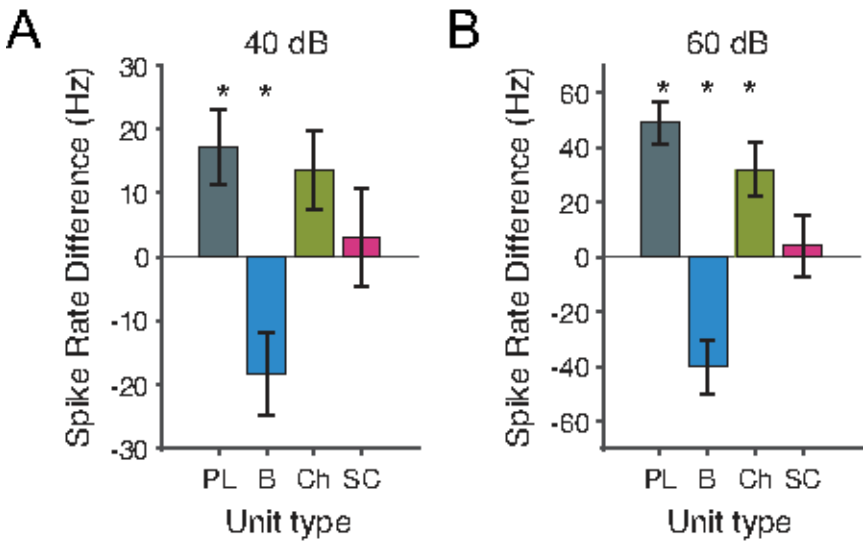

Fig 6: Quantification of small cell firing rates in background broadband noise (BBN) noise demonstrates maintenance of tone encoding. For a background sound level of either 40- (A) or 60- (B) dB SPL, the mean change in firing rate of each cell type between 60- and 90 dB SPL was calculated ($\alpha = 0.0125$, $p<0.05$; t-test with Bonferroni's correction).

Small cells display precise envelope coding

Tracking sound envelopes is important for decoding human speech or animal vocalizations (Shannon et al., 1995). Here, we used amplitude modulated broadband noise (75 dB SPL) to evaluate envelope coding in CN neurons. Figure 7 (A-C) shows an example vector strength calculation for a single SC at a modulation frequency of 32 Hz and depth of 12%, (Goldberg & Brown, 1969). This unit had a vector strength value of 0.43191, demonstrating accurate spike timing to the amplitude modulation. Figure 7 D shows that mean vector strength of the different VCN neurons peaked at a modulation frequency of 256 Hz, similar to that in previous studies (Sayles et al., 2013). At low modulation frequencies and depths, SCs had significantly greater vector-strength values than other VCN types (Fig 7) demonstrating superior envelope coding. The enhanced coding of low-frequency amplitude modulation in CN cells may be important for species-specific vocalization processing, as guinea pig vocalizations contain predominantly low frequency amplitude modulation bursts (Berryman, 1976).

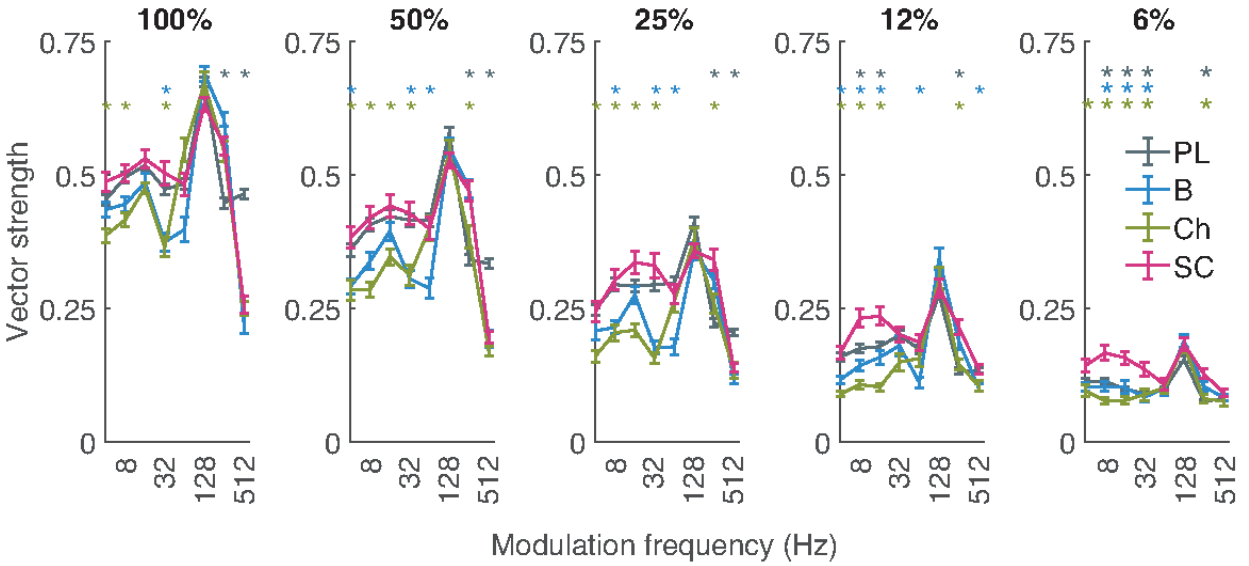

Fig 7: Small cells show more accurate amplitude-modulation coding than other CN cell types. Modulation transfer functions show vector strength of spiking to sinusoidally modulated BBN at 5 different modulation depths (100-6%). CN small cells have significantly greater vector strength of firing at modulation frequencies below 128 Hz and at lower modulation depths. Stars indicate significance between CN small cells and other cell types (One-way ANOVA with Tukey's multiple comparison test, $p<0.05$).

DISCUSSION

SCs receive exclusive afferent input from high-threshold, low/med SR ANFs, positioning them to encode sounds at levels well above threshold. Conversational speech (around 60 dB SPL) is encoded by temporal cues within amplitude modulated signals. Here, we showed that SCs encode both intensity and amplitude modulation with higher precision than other CN cell types. For tones in background noise, SCs were the only CN cell type that maintained coding above 60 dB SPL. The unique properties of SCs are likely mediated by cholinergic, MOC input to SCs, which provide excitation to SCs capable of overcoming the suppressive effect of MOCs on the cochlea, thereby increasing their suprathreshold firing rates.

SCs exhibited low SRs, high thresholds and steep, unsaturating (up to 90 dB SPL) rate-intensity slopes. These characteristics reflect the firing properties of the low/medium SR ANFs that innervate SCs and are similar to those identified in cells in the marginal region of the cat CN (Ghoshal & Kim, 1996, 1997). Those early studies also showed flat, bimodal or Unusual PSTH shapes, signifying a heterogenous population, similar to that shown here for guinea-pig CN SCs. However, in the present study, the difference between SC thresholds and other VCN cell types (~5 dB) was less than the threshold difference between low/medium and high SR ANFs (~20 dB; Liberman, 1978; Winter and Palmer, 1991), putatively due to the excitatory MOC cholinergic input to SCs demonstrated here. Blocking muscarinic, cholinergic receptors with atropine reduced SC spike rates while MOC stimulation, confirmed by CAP reductions, increased their firing rates. Both of these effects are consistent with the presence of excitatory cholinergic MOC input to the SCC. The greatest effect of blocking muscarinic cholinergic receptors was observed

during suprathreshold sound stimulation, which would be expected to also activate the sound-driven, cholinergic projections from MOC collaterals to the SCC (Lee et al., 2006).

MOC collaterals to the CN can influence other cell types (Baashar et al., 2019; Mulders et al., 2003, 2007) including T-stellate cells (planar multipolar cells with chopper responses) and D-stellate cells (radiate multipolar cells with onset chopper responses). Previous studies showed an increased firing rate in 94% of T-stellate cells following application of carbachol (AChR agonist) in vitro (Fujino & Oertel, 2001). However, Baashar et al. (2019) used tract tracing and double labelling to view contacts from MOC collaterals onto T- and D-stellate cells and demonstrated that MOC input to these CN cells had a weaker innervation pattern than would be expected based on the early electrophysiological studies. Some studies have suggested that there is inhibitory MOC projection to the CN (Mulders et al., 2002), however the present study found no evidence for inhibitory MOC or cholinergic effect on CN small cells or choppers. One possible reason for this discrepancy is the more targeted stimulation of contralateral MOC neurons in the present study, compared to midline stimulation, (Mulders et al., 2002), which would activate all crossed olivocochlear fibers including the lateral olivocochlear system.

The present data reveal strong, excitatory MOC-collateral innervation of SCs in the SCC but weak input to T-stellate cells. SC receptive fields in the present study had inhibitory sidebands, revealing a currently unknown source of inhibition. This is likely to be the glycinergic, D-stellate cells, which provide wideband inhibition to several cell types in the CN (Arnott et al., 2004; Oertel et al., 1990). However, further studies are required to confirm this pathway. An alternative source of inhibition is the L-stellate cell, which also responds to carbachol, suggesting cholinergic input, and thus potentially of olivocochlear origin (Ngodup et al., 2020). However, prediction of sources based on bath infusion of cholinergic modulators must be made with caution, due to multiple sources of cholinergic modulation to the CN (Mellott et al., 2011).

We demonstrated that SCs more accurately encode tones-in-noise compared to other CN cell types, putatively due to their restricted ANF inputs and unique input from MOC collaterals. Activating the MOC pathway to the cochlea suppresses the cochlear amplifier, benefitting speech-in-noise processing (de Boer et al., 2012; Winslow & Sachs, 1987). The function of MOC collaterals to the SCC may be to further aid speech coding. SCs have the characteristics necessary for superior suprathreshold sound encoding and accurately encode stimulus intensity (Figs 3&6). Pre-emptive MOC-pathway enhancement protects the cochlea from synaptopathic acoustic trauma (Boero et al., 2018), but whether increased MOC activation following synaptopathic noise exposure could reverse speech-in-noise deficits is still unknown. Conversely, in humans with tinnitus or hyperacusis, an increased contralateral suppression of otoacoustic emissions (Knudson et al., 2014) suggests an over-responsive MOC system in this pathology. MOC neurons are modulated by descending input from the inferior colliculus (Malmierca et al., 1996; Robertson & Mulders, 2000; Schofield & Cant, 1999), auditory cortex (Coomes & Schofield, 2004; Mulders & Robertson, 2000), and local inhibitory interneurons of the medial nucleus of the trapezoid body (Torres Cadenas et al., 2020). Descending modulation may be a route for auditory attention to affect peripheral processing, which may explain attentional facilitation of speech-in-noise understanding (de Boer et al., 2012). Descending modulation of MOC activity would also affect

MOC collateral input to CN SCs, which accurately encode intensity, providing an additional action pathway for auditory attention. The SCC in humans occupies a larger proportion of the CN than in rodents, and is therefore poised to play a major role in central mechanisms of speech perception (Moore & Osen, 1979).

Hearing damage in the absence of threshold shifts preferentially affects the higher threshold ANFs (Furman et al., 2013) that provide the sole afferent input to SCs. Cochlear synaptopathy is a potential major health issue in humans, as human temporal bones demonstrate widespread synaptic damage (Viana et al., 2015). One downstream effect of cochlear synaptopathy may be impaired speech perception, especially in the presence of background noise. This widespread complaint has been attributed to cochlear synaptopathy, but this relationship is still unclear (Plack et al., 2014). Human studies suggest that such perceptual deficits reflect difficulties in coding temporal envelopes (Bharadwaj et al., 2014), expected to impair speech recognition (Shannon et al., 1995). Temporal-coding deficits after synaptopathy are not apparent in ANFs (Heeringa et al., 2020), suggesting their origin may be central. The enhanced intensity coding and precise envelope coding shown here for SCs primes the SCC as an important subcortical area for speech processing is expected to be preferentially targeted by cochlear synaptopathy. In humans, the SCC occupies a large proportion of the CN and is therefore poised to play a major role in central mechanisms of auditory neuropathy (Moore & Osen, 1979). Speech coding in human SCs may be impaired following cochlear synaptopathy, and modulation of CN activity via the MOC pathway may be a potential treatment for the associated speech-in-noise deficits.

MATERIALS AND METHODS

All animal experimental procedures were performed in accordance with the protocols established by the National Institutes of Health (Publication 80-23) and approved by the University Committee on Use and Care of Animals at the University of Michigan. Male and female (n = 11 and 15, respectively) pigmented guinea pigs weighing 280-800g obtained from Elm Hill Labs were used. No differences in unit responses for animal's sex or age was found. Guinea pigs were dual-housed on a 12/12 h light-dark cycle, with food and water readily available. Auditory brainstem responses (ABRs) were used to confirm normal auditory thresholds of ≤20 dB SPL at 4-20kHz in all animals. ABRs (0–90 dB SPL tone bursts; 5 ms duration, 1 ms rise/fall times, 21 Hz presentation rate, 512 repetitions in 10 dB steps; Tucker-Davis Technologies RZ6) were recorded at 4, 8, 12, 16 and 20 kHz.

Surgery

Guinea pigs were initially anaesthetised with ketamine (50 mg kg^{-1}; Hospira Inc., Lake Forrest, IL, USA) and xylazine (5 mg kg^{-1}; Akorn Inc.; Lake Forrest, IL, USA). Anaesthetic depth was maintained using 10 mg kg^{-1} ketamine and 1 mg kg^{-1} xylazine supplements. Atropine (0.05 mg kg^{-1}) was administered during the initial surgery to reduce bronchial secretions. Animals were placed in a stereotaxic frame (Kopf; Tuijunga, U.S.A.) within a sound-attenuating and electrically shielded double-walled chamber. The skull was exposed, and a midline incision made, temporalis muscle removed, and a craniotomy performed to allow access to the left CN. The dura mater was removed and the exposed brain surface was kept moist by regular applications of saline.

Sound presentation

Auditory stimuli were delivered monaurally via a closed-field, calibrated system (modified DT770 drivers; Beyerdynamic Heilbronn, Germany) coupled to hollow ear bars. The speakers were driven by a Tucker-Davis Technologies (TDT; Alachua, FL, USA) System 3 (RZ6, PA5 & HB7), controlled by TDT Synapse and custom MATLAB 2021a (Mathworks; Natick, U.S.A) software.

Neural recordings

Multi-channel recording probes (NeuroNexus; Ann Arbor, MI, USA) were advanced stereotaxically through the cerebellum towards the left CN using an MP-285 microdrive (Sutter Instruments; Novato, CA, USA). Signals were amplified by a TDT PZ5 preamp connected to a TDT RZ2 processor for filtering (0.3 – 5 kHz), and data was collected using Synapse software. Spikes were detected on-line with threshold set at 4 standard deviations from mean background noise, then spike-sorted post-hoc using a PCA approach. Electrodes were positioned so that shanks spanned the DCN, SCC and AVCN. In 2 animals, electrode tracts were marked to confirm SCC positioning. Units were characterized by responses to tone-burst and BBN signals, also used to create receptive fields, PSTHs and RLFs (Ghoshal & Kim, 1997; Palmer, 1987; Stabler et al., 1996; Winter & Palmer, 1995), and divided into 4 categories; PL (bushy cells), Ch (T-stellates), SC (small cells) and B (buildups). Poorly driven units were discarded.

Rate-level function and intensity coding analyses

Receptive field stimuli consisted of randomized tonebursts (50 ms duration, 200 ms ISI, 0.1 octave spacing, 5 dB steps, 15 repeats, randomized). From these, threshold and BF were obtained from the lowest sound level to produce firing >2 standard deviations above spontaneous firing rates. RLFs at BF were then used for further analyses. Total inhibitory area of the receptive field was calculated as the number of squares of the receptive field where firing rate was <2 standard deviations below spontaneous firing rates.

For intensity coding, PSTH-based stimulus classification was performed using methods described in Foffani & Moxon (2004). Briefly, spike responses (serialized PSTH; 1 ms bins concatenated across units) of the neural population generated in each trial (50 trials total) were compared to the "template," or average PSTH, of a given stimulus intensity. Euclidean distances between each trial and the templates (19 total: 0 to 90 dB with 5 dB steps) were computed and the template with the shortest distance was then assigned as "classified intensity." Classification accuracy was defined as the percentage of trials that were classified within <10 dB of the actual intensity, or "hits." Coefficient of variation for classification result across all 50 trials was calculated as $\mathrm{std}(x^2)/\mathrm{mean}(x^2)$, where x counts the discretized step away from the "hit."

Drug delivery

Local drug delivery of the muscarinic acetylcholine receptor antagonist, atropine was achieved using a NeuroNexus D16 puffer-probe. The probe was connected to a 100 µl syringe containing an 80 µM solution. The syringe was fixed to a digital syringe driver (UMP3 microsyringe injector with Micro4 controller; World Precision Instruments; Sarasota, FL). This system allows simultaneous drug delivery and neural recordings as described and validated in previous studies (Rohatgi et al., 2009; Stefanescu & Shore, 2015, 2017). After assessing baseline CN neuronal activity, 2 µl of solution was delivered at a rate of 100 nl/min, as in previous studies (Rohatgi et al., 2009; Stefanescu & Shore, 2015, 2017).

Round window recordings

Cochlear compound action potential (CAP) recordings were performed using an insulated silver-wire ball inserted through the bulla to rest on the cochlear round window. The trailing wire was sealed to the skull, with a small hole left open for fluid wicking. CAPs were recorded in response to 10 ms tones with rise/fall times of 2 ms. Amplitudes were calculated as P_1-N_1 of the mean CAP waveform (200 repeats).

Electrical stimulation

MOC neurons in the VNTB were electrically stimulated with biphasic current pulses (100 ms duration, 0.1 ms pulse width, 100 Hz, 500-1000 µA; 5/sec) applied through concentric bipolar electrodes (CBCEF75; FHC; Bowdoin, ME). CAPs were recorded to verify MOC neuron location (16 kHz, 70 dB SPL tone). CAP amplitudes were compared at baseline and 5 ms after the cessation of electrical stimulation. A CAP-amplitude reduction of >30% confirmed accurate MOC locations in the VNTB for stimulation. Current levels were titrated to ensure maximal MOC activation with no elicited muscular contractions.

Imaging

In a separate guinea pig, a tract tracing experiment was performed to confirm VNTB projections to and from SCC. FluroEmerald (10%; 0.5 µl, Thermo Fisher Scientific, Waltham, MA, USA) was pressure-injected (0.1 µl min-1) into the contralateral VNTB (1 mm anterior to the interaural line, 1.5 mm lateral to midline, 12 mm from the dural surface). The animal was anesthetised with ketamine-xylazine mixture in the same manner as described for electrophysiology experiments but allowed to recover and maintained in the vivarium for 5 days before transcardial perfusion (100 mL 1× PBS, 400 mL 4% paraformaldehyde) after euthanasia. The brain was extracted, post-fixed for 2 h, immersed in 30% sucrose solution for 2 days, frozen and cryosectioned at 50 µm in the coronal plane (Leica, CM3050S). Coverslipped brain sections were examined under confocal epifluorescence (PMT; Leica, SP5-x).

Experimental design and statistical analysis

SC sound evoked responses were compared to other CN cell types. Changes in these responses during MOC modulation were also analysed. Statistical tests, including Kruskal-Wallis test, ANCOVA, and two-way ANOVA were used to compare between cell-types or conditions (α = 0.05). Post hoc analyses were performed using Tukey's multiple comparison test.

REFERENCES

Arnott, R. H., Wallace, M. N., Shackleton, T. M., & Palmer, A. R. (2004). Onset Neurones in the Anteroventral Cochlear Nucleus Project to the Dorsal Cochlear Nucleus. *Journal of the Association for Research in Otolaryngology*, *5*(2), 153–170.

Baashar, A., Robertson, D., Yates, N. J., & Mulders, W. H. A. M. (2019). Targets of Olivocochlear Collaterals in Cochlear Nucleus of Rat and Guinea Pig. *Journal of Comparative Neurology*, *527*(March), 2273–2290.

Benson, T. E., Berglund, A. M., & Brown, M. C. (1996). Synaptic input to cochlear nucleus dendrites that receive medial olivocochlear synapses. *Journal of Comparative Neurology*, *365*(1), 27–41.

Benson, T. E., & Brown, M. C. (1990). Synapses formed by olivocochlear axon branches in the mouse cochlear nucleus. *The Journal of Comparative Neurology*, *295*(1), 52–70.

Berryman, J. C. (1976). Guinea-pig Vocalizations: Their Structure, Causation and Function. *Zeitschrift Für Tierpsychologie*, *41*(1), 80–106. https://doi.org/10.1111/j.1439-0310.1976.tb00471.x

Bharadwaj, H. M., Verhulst, S., Shaheen, L., Liberman, M. C., Shinn-Cunningham, B. G., Peelle, J. E., Léger, A. C., & Elisabeth Gockel, H. (2014). Cochlear neuropathy and the coding of supra-threshold sound. *Frontiers in Systems Neuroscience*, *8*(26).

Boero, L. E., Castagna, V. C., Di Guilmi, M. N., Goutman, J. D., Elgoyhen, A. B., & Gómez-Casati, M. E. (2018). Enhancement of the Medial Olivocochlear System Prevents Hidden Hearing Loss. *Journal of Neuroscience*, *38*(34), 7440–7451.

Cant, N. B. (1993). The Synaptic Organization of the Ventral Cochlear Nucleus of the Cat: The Peripheral Cap of Small Cells. In *The Mammalian Cochlear Nuclei* (pp. 91–105). Springer US.

Coomes, D. L., & Schofield, B. R. (2004). Projections from the auditory cortex to the superior olivary complex in guinea pigs. *European Journal of Neuroscience*, *19*(8), 2188–2200. https://doi.org/10.1111/j.0953-816X.2004.03317.x

Darrow, K. N., Benson, T. E., & Brown, M. C. (2012). Planar multipolar cells in the cochlear nucleus project to medial olivocochlear neurons in mouse. *The Journal of Comparative Neurology*, *520*(7), 1365–1375.

de Boer, J., Thornton, A. R. D., & Krumbholz, K. (2012). What is the role of the medial olivocochlear system in speech-in-noise processing? *Journal of Neurophysiology*, *107*(5), 1301–1312.

De Venecia, R. K., Liberman, M. C., Guinan, J. J., & Brown, M. C. (2005). Medial olivocochlear reflex interneurons are located in the posteroventral cochlear nucleus: A kainic acid lesion study in guinea pigs. *Journal of Comparative Neurology*, *487*(4), 345–360.

Dolan, D. F., & Nuttall, A. L. (1988). Masked cochlear whole-nerve response intensity functions altered by electrical stimulation of the crossed olivocochlear bundle. *J. Acoust. Soc. Am*, *83*(3), 1081–1086.

Foffani, G., & Moxon, K. A. (2004). PSTH-based classification of sensory stimuli using ensembles of single neurons. *Journal of Neuroscience Methods*, *135*(1–2), 107–120. https://doi.org/10.1016/j.jneumeth.2003.12.011

Fujino, K., & Oertel, D. (2001). Cholinergic modulation of stellate cells in the mammalian ventral

cochlear nucleus. *Journal of Neuroscience*, *21*(18), 7372–7383.

Furman, A. C., Kujawa, S. G., & Liberman, M. C. (2013). Noise-induced cochlear neuropathy is selective for fibers with low spontaneous rates. *Journal of Neurophysiology*, *110*(3), 577–586.

Ghoshal, S., & Kim, D. O. (1996). Marginal shell of the anteroventral cochlear nucleus: intensity coding in single units of the unanesthetized, decerebrate cat. *Neuroscience Letters*, *205*, 71–74.

Ghoshal, S., & Kim, D. O. (1997). Marginal Shell of the Anteroventral Cochlear Nucleus: Single-Unit Response Properties in the Unanesthetized Decerebrate Cat. *J Neurophysiol*, *77*(4), 2083–2097.

Goldberg, J. M., & Brown, P. B. (1969). Response of Binaural Neurons of Dog Superior Olivary Complex to Dichotic Tonal Stimuli: Some Physiological Mechanisms of Sound Localization. *American Physiological Society*, *32*(4), 613–636.

Heeringa, A. N., Zhang, L., Ashida, G., Beutelmann, R., Steenken, F., & Köppl, C. (2020). Temporal Coding of Single Auditory Nerve Fibers Is Not Degraded in Aging Gerbils. *The Journal of Neuroscience : The Official Journal of the Society for Neuroscience*, *40*(2), 343–354.

Kawase, T., & Liberman, M. C. (1993). Antimasking Effects of the Olivocochlear Reflex. I. Enhancement of Compound Action Potentials to Masked Tones. *Journal of Physiology*, *70*(6).

Knudson, I. M., Shera, C. A., & Melcher, J. R. (2014). Increased contralateral suppression of otoacoustic emissions indicates a hyperresponsive medial olivocochlear system in humans with tinnitus and hyperacusis. *Journal of Neurophysiology*, *112*(12), 3197–3208.

Kujawa, S. G., Glattke, T. J., Fallon, M., & Bobbin, R. P. (1993). Contralateral sound suppresses distortion product otoacoustic emissions through cholinergic mechanisms. *Hearing Research*, *68*(1), 97–106. https://doi.org/10.1016/0378-5955(93)90068-C

Lee, D. J., De Venecia, R. K., Guinan, J. J., & Brown, M. C. (2006). Central auditory pathways mediating the rat middle ear muscle reflexes. *Anatomical Record - Part A Discoveries in Molecular, Cellular, and Evolutionary Biology*, *288*(4), 358–369. https://doi.org/10.1002/ar.a.20296

Liberman, M. C. (1978). Auditory-nerve response from cats raised in a low-noise chamber. *The Journal of the Acoustical Society of America*, *63*, 442.

Liberman, M. C. (1991). Central projections of auditory-nerve fibers of differing spontaneous rate. I. Anteroventral cochlear nucleus. *Journal of Comparative Neurology*, *313*(2), 240–258.

Malmierca, M. S., Le Beau, F. E. N., & Rees, A. (1996). The topographical organization of descending projections from the central nucleus of the inferior colliculus in guinea pig. *Hearing Research*, *93*(1–2), 167–180.

Mellott, J. G., Motts, S. D., & Schofield, B. R. (2011). Multiple origins of cholinergic innervation of the cochlear nucleus. *Neuroscience*, *180*, 138–147.

Moore, J. K., & Osen, K. K. (1979). The cochlear nuclei in man. *American Journal of Anatomy*, *154*(3), 393–417.

Mulders, W. H. A. M., Harvey, A. R., & Robertson, D. (2007). Electrically Evoked Responses in Onset Chopper Neurons in Guinea Pig Cochlear Nucleus. *Journal of Neurophysiology*, *97*(5),

527 3288–3297.
528 Mulders, W. H. A. M., Paolini, A. G., Needham, K., & Robertson, D. (2003). Olivocochlear
529 collaterals evoke excitatory effects in onset neurones of the rat cochlear nucleus. *Hearing*
530 *Research*, *176*(1–2), 113–121.
531 Mulders, W. H. A. M., & Robertson, D. (2000). Evidence for direct cortical innervation of medial
532 olivocochlear neurones in rats. *Hearing Research*, *144*(1–2), 65–72.
533 https://doi.org/10.1016/S0378-5955(00)00046-0
534 Mulders, W. H. A. M., Winter, I. M., & Robertson, D. (2002). Dual action of olivocochlear
535 collaterals in the guinea pig cochlear nucleus. *Hearing Research*, *174*(1–2), 264–280.
536 https://doi.org/10.1016/S0378-5955(02)00701-3
537 Ngodup, T., Romero, G. E., & Trussell, L. O. (2020). Identification of an inhibitory neuron
538 subtype, the l-stellate cell of the cochlear nucleus. *ELife*, *9*, 1–40.
539 https://doi.org/10.7554/eLife.54350
540 Oertel, D., Wu, S. H., Garb, M. W., & Dizack, C. (1990). Morphology and physiology of cells in
541 slice preparations of the posteroventral cochlear nucleus of mice. *Journal of Comparative*
542 *Neurology*, *295*(1), 136–154.
543 Palmer, A. R. (1987). Physiology of the cochlear nerve and cochlear nucleus. *Br Med Bull*, *43*(4),
544 838–855.
545 Pichora-Fuller, M. K. (1997). Language comprehension in older listeners. *Journal of Speech-*
546 *Language Pathology and Audiology*, *21*(2), 125–142. https://psycnet.apa.org/record/1997-
547 05664-003
548 Plack, C. J., Barker, D., & Prendergast, G. (2014). Perceptual Consequences of "Hidden" Hearing
549 Loss. *Trends in Hearing*, *18*, 1–11.
550 Robertson, D., & Mulders, W. H. A. M. (2000). Distribution and possible functional roles of some
551 neuroactive peptides in the mammalian superior olivary complex. *Microscopy Research*
552 *and Technique*, *51*(4), 307–317.
553 Rohatgi, P., Langhals, N. B., Kipke, D. R., & Patil, P. G. (2009). In vivo performance of a
554 microelectrode neural probe with integrated drug delivery. *Neurosurg Focus*, *27*(1), 8.
555 Ryan, A. F., Keithley, E. M., Wang, Z. -X, & Schwartz, I. R. (1990). Collaterals from lateral and
556 medial olivocochlear efferent neurons innervate different regions of the cochlear nucleus
557 and adjacent brainstem. *Journal of Comparative Neurology*, *300*(4), 572–582.
558 Ryugo, D. K. (2008). Projections of low spontaneous rate, high threshold auditory nerve fibers
559 to the small cell cap of the cochlear nucleus in cats. *Neuroscience*, *154*(1), 114–126.
560 Sayles, M., Füllgrabe, C., & Winter, I. M. (2013). Neurometric amplitude-modulation detection
561 threshold in the guinea-pig ventral cochlear nucleus. *The Journal of Physiology*
562 *Neuroscience C*, *591*(13), 3401–3419.
563 Schofield, B. R., & Cant, N. B. (1999). Descending auditory pathways: Projections from the
564 inferior colliculus contact superior olivary cells that project bilaterally to the cochlear
565 nuclei. *Journal of Comparative Neurology*, *409*(2), 210–223.
566 Schofield, B. R., Mellott, J. G., & Motts, S. D. (2014). Subcollicular projections to the auditory
567 thalamus and collateral projections to the inferior colliculus. *Frontiers in Neuroanatomy*,
568 *8*(70), 1–16.
569 Schofield, B. R., Motts, S. D., Mellott, J. G., & Foster, N. L. (2014). Projections from the dorsal
570 and ventral cochlear nuclei to the medial geniculate body. *Frontiers in Neuroanatomy*,

571 *8*(10), 1–12.
572 Shannon, R. V, Zeng, F., Kamath, V., Wygonski, J., & Ekelid, M. (1995). Speech Recognition with
573 Primarily Temporal Cues. *Science*, *270*(5234), 303–304.
574 Stabler, S. E., Palmer, A. R., & Winter, I. M. (1996). Temporal and mean rate discharge patterns
575 of single units in the dorsal cochlear nucleus of the anesthetized guinea pig. *Journal of*
576 *Neurophysiology*, *76*(3), 1667–1688.
577 Stefanescu, R. A., & Shore, S. E. (2015). NMDA receptors mediate stimulus-timing-dependent
578 plasticity and neural synchrony in the dorsal cochlear nucleus. *Frontiers in Neural Circuits*,
579 *9*(November), 1–14.
580 Stefanescu, R. A., & Shore, S. E. (2017). Muscarinic acetylcholine receptors control baseline
581 activity and hebbian stimulus timing-dependent plasticity in fusiform cells of the dorsal
582 cochlear nucleus. *Journal of Neurophysiology*, *117*(3), 1229–1238.
583 Thompson, A. M., & Thompson, G. C. (1991). Posteroventral cochlear nucleus projections to
584 olivocochlear neurons. *The Journal of Comparative Neurology*, *303*(2), 267–285.
585 Torres Cadenas, L., Matthew, X., Fischl, J., & Weisz, C. J. C. (2020). Synaptic Inhibition of Medial
586 Olivocochlear Efferent Neurons by Neurons of the Medial Nucleus of the Trapezoid Body.
587 *The Journal of Neuroscience*, *40*(3), 509–525.
588 Viana, L. M., O, J. T., Burgess, B. J., Jones, D. D., ACP Oliveira, C., Santos, F., Merchant, S. N.,
589 Liberman, L. D., & Charles Liberman, M. (2015). Cochlear neuropathy in human
590 presbycusis: confocal analysis of hidden hearing loss in post-mortem tissue HHS Public
591 Access. *Hear Res*, *327*, 78–88. https://doi.org/10.1016/j.heares.2015.04.014
592 Winslow, R. L., & Sachs, M. B. (1987). Effect of Electrical Stimulation of the Crossed
593 Olivocochlear Bundle on Auditory Nerve Response to Tones in Noise. *Journal of*
594 *Neurophysiology*, *57*(4), 1002–1021.
595 Winter, I. M., & Palmer, A. R. (1991). Intensity coding in low-frequency auditory-nerve fibers of
596 the guinea pig. *The Journal of the Acoustical Society of America*, *90*(4), 1958–1967.
597 Winter, I. M., & Palmer, A. R. (1995). Level dependence of cochlear nucleus onset unit
598 responses and facilitation by second tones or broadband noise. *Journal of*
599 *Neurophysiology*, *73*(1), 141–159.
600 Ye, Y., Machado, D. G., & Kim, D. O. (2000). Projection of the marginal shell of the anteroventral
601 cochlear nucleus to olivocochlear neurons in the cat. *The Journal of Comparative*
602 *Neurology*, *420*(1), 127–138.
603 Young, E. D., Robert, J. M., & Shofner, W. P. (1988). Regularity and latency of units in ventral
604 cochlear nucleus: implications for unit classification and generation of response properties.
605 *Journal of Neurophysiology*, *60*(1), 1–29.

606

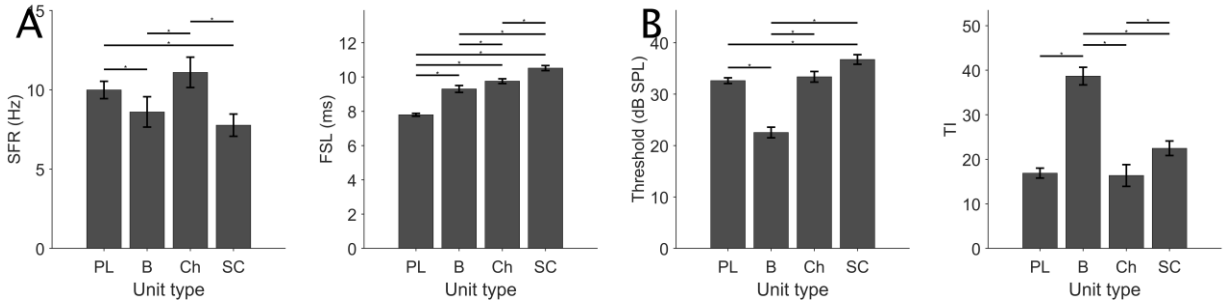

Fig S1: Small cells show lower SFRs and longer FSLs than other VCN units. A) Bar plot (mean ± SEM) of SFR for CN cell types (primary-like (PL), chopper (Ch), small cell (SC) and buildup. B) Bar plot (mean ± SEM) for FSL. C) Bar plot (mean ± SEM) of thresholds for each CN cell type. D) Bar plot (mean ± SEM) of total inhibitory (TI) area of the receptive field. Comparisons between groups were made using a Kruskal-Wallis test with Tukey's multiple comparison test *p<0.05.